Journal of the Mechanics and Physics of Solids 60 (2012) 1447–1461

Contents lists available at SciVerse ScienceDirect

Journal of the Mechanics and Physics of Solids

journal homepage: www.elsevier.com/locate/jmps

Study on the mechanisms and quantitative law of mode I supersonic crack propagation

Y.J. Jia [a], W.P. Zhu [a], T. Li [b], B. Liu [a,*]

[a] AML, CNMM, Department of Engineering Mechanics, Tsinghua University, Beijing 100084, China
[b] Department of Mechanical Engineering, University of Maryland, College Park, MD 20742, USA

ARTICLE INFO

Article history:
Received 2 December 2011
Received in revised form
17 April 2012
Accepted 20 April 2012
Available online 7 May 2012

Keywords:
Dynamic fracture
Supersonic crack propagation
Discrete systems

ABSTRACT

Continuum mechanics predicts that the propagation speed of non-equilibrium information in solids is limited by the longitudinal wave speed, so is crack propagation. However, solids are essentially discrete systems. In this paper, via theoretical analysis and numerical simulations, it is demonstrated in a straightforward way that non-equilibrium disturbance (e.g. force, displacement, energy, and so on) can propagate at a supersonic speed in discrete systems, although the magnitude of the disturbance attenuates very quickly. In dynamic fracture, a cascade of atomic-bond breaking events provides an amplification mechanism to counterbalance the attenuation of the disturbance. Therefore, supersonic crack propagation can be realized in a domino way. Another key factor for supersonic crack propagation is to ensure sufficient energy flowing into the crack tip. Since most energy can only be transferred at a speed limited by the longitudinal wave speed, the conditions for the occurrence of supersonic crack propagation are not easily met in most situations, unless there is high pre-stored energy along the crack path or continuous energy supply from the loading concomitantly moving with the crack tip. A quantitative relation between supersonic crack propagation speed and material properties and parameters is given, which implies that knowing all the classical macroscopic quantities is not enough in determining the supersonic crack propagation speed, and the microstructure does play a role. Moreover, it is interesting to note that fracture toughness affects the crack propagation speed in the subsonic regime, but not in the supersonic regime, because the deformation/stress is uniform in front of a supersonic crack where strength criterion dominates.

1. Introduction

Rapidly propagating crack has been studied for many years, but lots of phenomena have still not been understood thoroughly. Especially, what is the upper limit of crack propagation speed attracts much attention recently, and there is a lack of consensus on the answer to this question. In the framework of continuum mechanics, dynamic fracture mechanics predicts that the energy release rate for mode I crack becomes negative if the crack propagates faster than the Rayleigh wave speed, implying that the Rayleigh wave speed is the upper limit of mode I crack speed (Broberg, 1999; Freund, 1998; Slepyan, 2002). Previous numerical simulations (Abraham et al., 1994, 1997; Buehler et al., 2004b; Rountree, 2002; Swadener et al., 2002) and experimental work (Cramer et al., 2000; Fineberg et al., 1991; Hauch et al., 1999; Hauch and

* Corresponding author. Tel.: +86 10 62786194; fax: +86 10 62781824.
E-mail address: liubin@tsinghua.edu.cn (B. Liu).

0022-5096/$ - see front matter © 2012 Elsevier Ltd. All rights reserved.
http://dx.doi.org/10.1016/j.jmps.2012.04.008

Marder, 1998; Marder and Gross, 1995; Ravi-Chandar, 1998) showed that crack does not propagate beyond the Rayleigh wave speed. For a mode II crack, continuum mechanics also predicts a negative energy release rate if the crack propagates faster than the Rayleigh wave speed, except in the range of intersonic propagation (between the shear and longitudinal wave speeds), which implies that a mode II crack can propagate at intersonic speed. Burridge (1973) attributed the mechanism to the positive peak of shear stress ahead of the tip of the mode II crack tip traveling at the Rayleigh wave speed. Andrews (1976) found that when the speed of crack propagation approaches to the Rayleigh wave speed, a microcrack with the velocity beyond the shear wave speed will be induced ahead of the mother crack tip. Taking advance of molecular dynamics (MD) method, Abraham and Gao et al. (Abraham and Gao, 2000; Gao, 2001; Abraham, 2001) simulated the mode II crack propagation at the velocity exceeding shear wave speed and found a daughter crack formed ahead of the mother crack tip. Needleman (1999) obtained the similar results using the cohesive surface in finite element simulations. The experimental observation of Rosakis et al. (1999; 2002) provided the first direct evidence that a mode II crack can travel at intersonic speed.

However, it is also noted that continuum mechanics fails to predict the following numerical and experiments results on dynamic fracture. Gao (1997) and Abraham (1996, 1997) observed in their MD simulations that a mode I crack propagates at super-Rayleigh speed, and a mode II crack propagates at supersonic speed. They attributed the phenomenon to the local hyperelastic effects of solids (Buehler et al., 2003, 2004a; Buehler and Gao, 2006; Guo et al., 2003). Also using MD method to investigate dynamic fracture, Guozden et al. (2005; 2010) concluded that both mode I and mode III cracks can propagate at supersonic speed. Petersan et al. (2004) conducted dynamic fracture experiments on popping rubber, and found that the crack propagation speed of a mode I crack is faster than the shear wave speed. Slepyan (1972, 1981, 2001a, 2001b) pioneered the theoretical study on the possibility of supersonic crack propagation in lattice system and presented the corresponding analytical solutions. Adopting similar theoretical analyses, Mishuris et al. (2008, 2009) studied the bridge crack propagation in lattice system and found that the supersonic crack propagation speed was predicted in the analytical results.

The contradiction between the predictions from continuum mechanics and those from experimental and MD results on the upper limit of crack propagation speed has brought a lot of confusion. On the one hand, according to continuum mechanics theory, any information of non-equilibrium disturbance cannot travel faster than the longitudinal wave speed. If so, how can a crack propagate faster than this upper limit speed? On the other hand, the MD simulations and experiments indeed demonstrated that the Rayleigh wave speed, or even the longitudinal wave speed, can be exceeded in mode I crack propagation. These contradictive predictions inspire us to suspect that the essential discreteness of solids might play an important role in rapid dynamic fracture, which is neglected or smeared out in continuum mechanics. We would like to emphasize that all solids consist of discrete atoms, and continuum mechanics is only an idealized model of solids based on continuity assumption. In most cases, continuum mechanics can give good predictions and have been widely used. However, the fracture of solids involves atomic bond breaking at the crack tip, and continuum mechanics might yield incorrect predictions in certain extreme cases.

This paper is aimed to explore the underlying mechanisms of supersonic crack propagation, and study the quantitative dependence of supersonic crack propagation speed on both material properties and microstructure parameters. The structure of this paper is as follows. In Section 2, we show several numerical cases in which a mode I crack propagates at a supersonic speed. In Section 3, by investigating the difference between the dynamic behaviors of one dimensional discrete and continuous solid system, we demonstrate that the information of non-equilibrium disturbance can propagate at a supersonic speed, which is the key factor validating the possibility of supersonic propagation of a mode I crack. In Section 4, we investigate several typical loading conditions, and reveal suitable energy supply mechanisms for maintaining supersonic crack propagation. In Section 5, the effects of microstructure and other parameters on supersonic crack propagation are discussed. Conclusions are summarized in Section 6.

2. Numerical examples of supersonic mode I crack propagation

To systematically study the dynamic fracture behaviors, a two-dimensional strip specimen with triangle lattice shown in Fig. 1a is simulated. This is an idealized model for a solid crystal, in which concentrated mass m is only deployed at nodes (or atoms) and the connecting bonds are represented by massless linear springs with original length l_0 and spring constant k. The simulation system consists of 120 rows, and each row has 450 nodes. At first, vertical tensile displacement loading is applied to the top and bottom boundaries of the non-cracked specimen, and the system is under uniform deformation with stretched bond length l_a. A crack is then suddenly introduced by removing the left part of bonds crossing the horizontal middle plane while keeping the displacement loading fixed as shown in Fig. 1a. In order to simulate a straight propagating crack, it is assumed that the rest of the bonds crossing this middle plane (colored by red) have a critical breaking length l_c, while the other bonds never break. The dynamical finite element method (FEM) (ABAQUS, 2005) is used to simulate the subsequent dynamic fracture behaviors. The focus of this numerical study is to investigate whether a mode I crack can propagate at a supersonic speed.

We first determine the longitudinal wave speed of this two dimensional network by simulation and theoretical analysis. Fig. 2a shows three sequential snapshots of the non-cracked specimen after a pulse dilatational loading on the left part of the specimen, from which the longitudinal wave speed can be computed as $c_l = 1.061 l_0 \sqrt{k/m}$. The following theoretical analysis further validates this computed value. According to continuum mechanics, the elastic constants of a

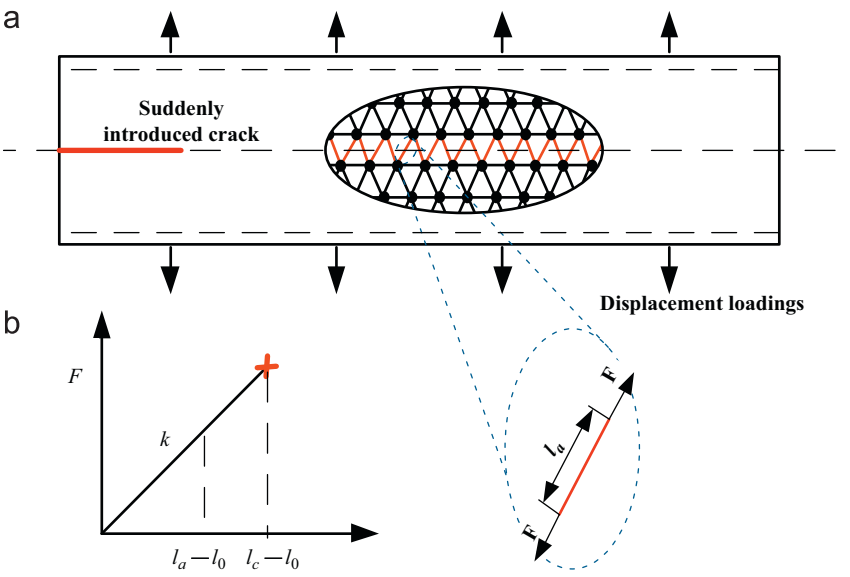

Fig. 1. (a) The simulation model of a two-dimensional strip specimen with triangle lattice. The red bonds crossing the middle plane are assumed to be weak with a critical force-stretch curve (b) (For interpretation of the references to color in this figure legend, the reader is referred to the web version of this article.).

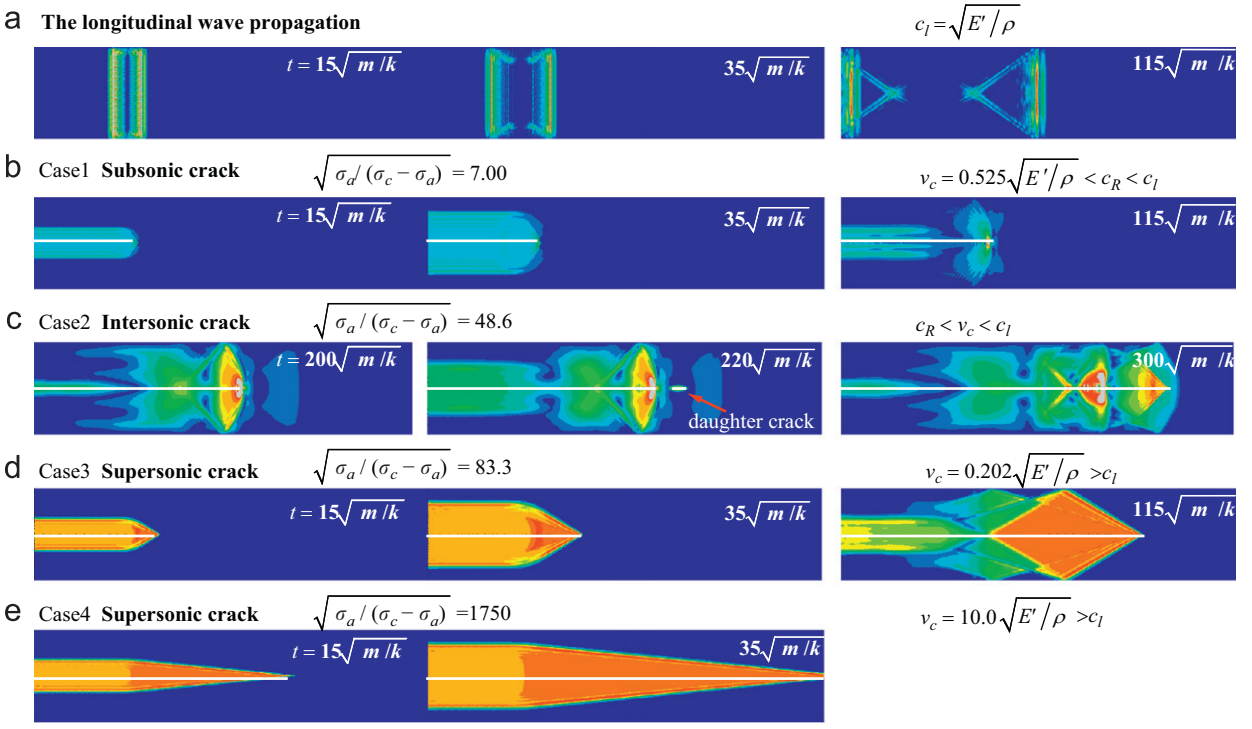

Fig. 2. Sequential snapshots of the propagation of longitudinal wave (a) and dynamical crack for pre-stretched strip specimen with different critical breaking bond lengths, $\sqrt{\sigma_a/(\sigma_c - \sigma_a)} = 7.00$(b),48.6(c),83.3(d) and 1750(e), respectively. Color shades denote nodal speed.

two dimensional triangular lattice behaving as a plane stress strip can be depicted as (Gao, 1996)

$$\mu = \frac{\sqrt{3}}{4}k, \quad E = \frac{2}{\sqrt{3}}k, \quad \nu = \frac{1}{3} \tag{1}$$

where μ is the shear modulus, E is the Young's modulus and ν is the Poisson's ratio. The density of the triangular lattice is

$$\rho = \frac{2m}{\sqrt{3}{l_0}^2} \tag{2}$$

Therefore, its longitudinal wave speed is

$$c_l = \sqrt{\frac{E}{(1-\nu^2)\rho}} = l_0\sqrt{\frac{9k}{8m}} \approx 1.061 l_0\sqrt{\frac{k}{m}} \tag{3}$$

The consistency of the computed value with the theoretical prediction verifies the simulation approach. For convenience, we introduce the nominal modulus as

$$E' = \frac{E}{(1-\nu^2)} \tag{4}$$

which represents the tensile stiffness of the material without lateral shrinkage. The longitudinal wave speed can be rewritten as

$$c_l = \sqrt{\frac{E'}{\rho}} \tag{5}$$

Moreover, the Rayleigh wave speed is

$$c_R \approx 0.566 l_0\sqrt{\frac{k}{m}} \approx 0.534\sqrt{\frac{E'}{\rho}} \tag{6}$$

We then simulate four cases with various dynamic fracture behaviors. For consistency, the pre-stretched bond length in all cases is fixed as $l_a = 1.008745 l_0$, and the critical breaking bond length l_c is reduced case by case, which makes the crack propagate more easily and faster. We also use σ_a and σ_c to represent the pre-stress and strength of the system, respectively, and

$$\begin{aligned} \sigma_a &= \frac{4E'}{3}\frac{l_a - l_0}{l_0} \\ \sigma_c &= \frac{4E'}{3}\frac{l_c - l_0}{l_0} \end{aligned} \tag{7}$$

Case 1. (*Subsonic crack propagation*). Fig. 2b shows simulation Case 1 with $\sigma_a/(\sigma_c-\sigma_a)=(l_a-l_0)/(l_c-l_a)=7.00$ in which the crack propagation speed is slower than the longitudinal wave speed c_l and the Rayleigh wave speed c_R. This case falls into the predictable regime of continuum fracture mechanics.

Case 2. (*Intersonic crack propagation*). Fig. 2c shows simulation case 2 with a lower l_c so that $\sigma_a/(\sigma_c-\sigma_a)=(l_a-l_0)/(l_c-l_a)=48.6$. In this case, the daughter crack is formed in front of the mother crack tip and propagates faster than c_R, and similar phenomena have been reported and investigated in previous studies on mode II crack (Abraham and Gao, 2000). However, different from the case of mode II shear crack, the nucleation of the daughter crack in our modeling is due to the longitudinal wave reflection against the boundary and meeting ahead of the mother crack. This regime cannot be understood and predicted by continuum fracture mechanics on mode I crack.

Case 3 and 4. (*Supersonic crack propagation*). Further reducing l_c, so that $\sigma_a/(\sigma_c-\sigma_a)=(l_a-l_0)/(l_c-l_a)=83.3$ in case 3 and $\sigma_a/(\sigma_c-\sigma_a)=(l_a-l_0)/(l_c-l_a)=1750$ in case 4, it is found that the crack can propagate at a supersonic speed, namely faster than the longitudinal wave speed, as clearly shown by the Mach cones in Fig. 2d and e. It is also noted that when the critical breaking bond length l_c approaches the pre-stretched bond length l_a (or the strength σ_c approaches the pre-stress σ_a), the crack can propagate much faster than the longitudinal wave speed (e.g., roughly 10 times faster in case 4). This can be understood by an extreme case: when l_c equals to l_a (or σ_c equals to σ_a), all bonds reach their strength simultaneously, i.e. the crack propagates at an infinite speed. The continuum fracture mechanics is not capable of predicting this regime either.

It should be pointed out that all simulations above have been further verified by another numerical approach, molecular dynamics, and the convergence of time step is also checked. Therefore, we are confident on the simulation results of supersonic crack propagation. The contradiction between our simulation results and continuum fracture mechanics on the upper limit of crack propagation speed inspires us to suspect that some features of dynamic fracture might be lost by the continuity assumption. In particular, two underlying mechanisms are of our concerns

1) The longitudinal wave speed has been believed as an upper limit speed in continuum mechanics. How can a non-equilibrium disturbance propagate faster than it?
2) How is the energy pre-stored or supplied to maintain continuous supersonic crack propagation?

These two issues will be discussed in the following two sections separately.

3. The supersonic propagation of non-equilibrium disturbance in discrete systems

For simplicity, one dimensional discrete mass-spring system shown in Fig. 3a is adopted to investigate its dynamic response. Identical to the previous example in Section 2, the springs are massless with spring constant k and original length l_0. Each node has a concentrated mass m. A half-length spring with spring constant $2k$ is deployed at the right end for future convenience. This system is stress free at the initial time $t=0$. We then suddenly impose a constant velocity load $v_0 = l_0\sqrt{k/m}$ at the right end. According to continuum mechanics, this disturbance will propagate at the longitudinal speed $c_l = \sqrt{E/\rho} = l_0\sqrt{k/m}$, and two adjacent nodes will sense this disturbance with a time interval $\Delta t_{continuum} = l_0/c_l = \sqrt{m/k}$. For comparison, we will investigate if the corresponding time interval of this discrete system is less than $\Delta t_{continuum}$ via direct simulation.

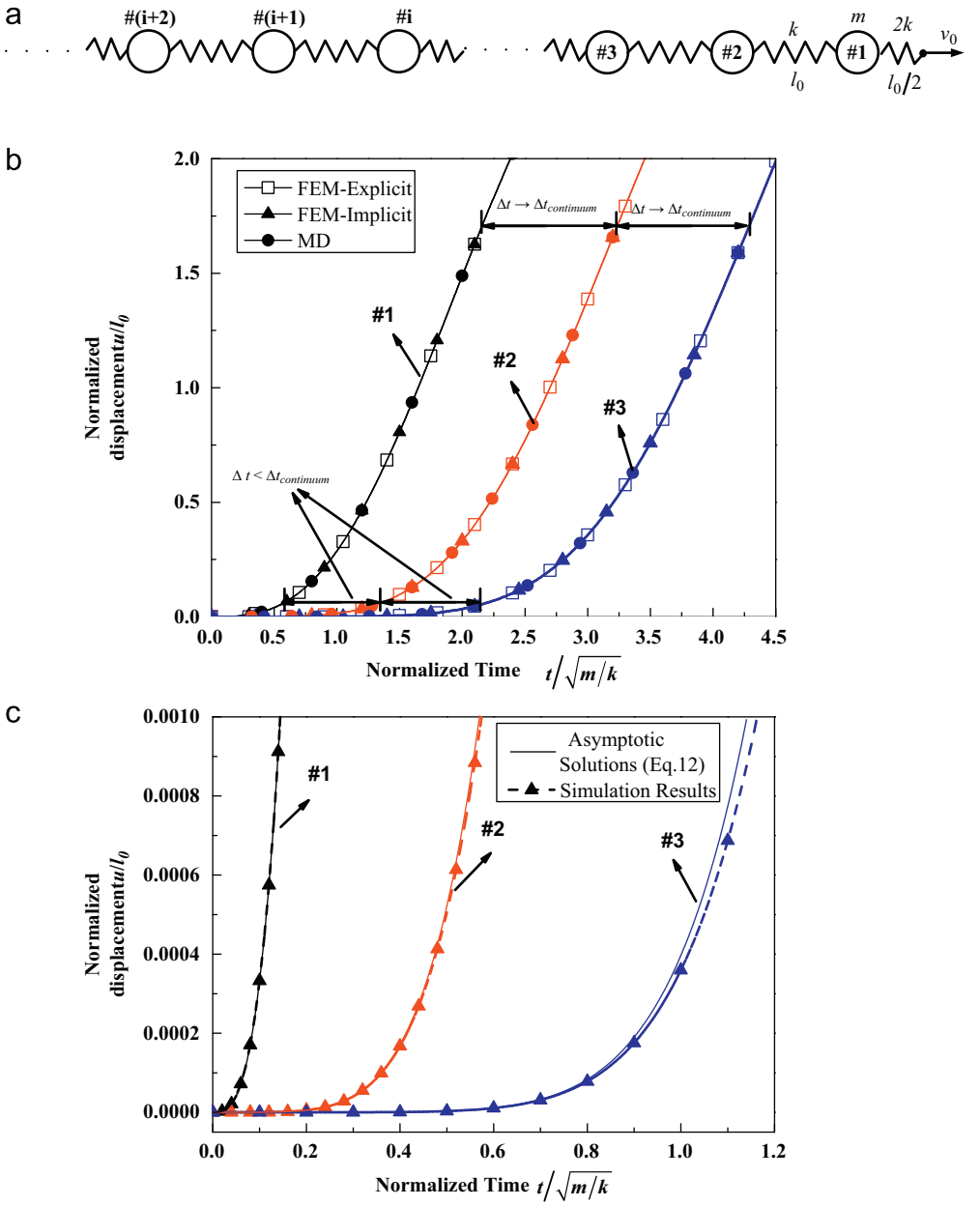

Fig. 3. (a) Schematic of a one dimensional discrete mass-spring system subjected to a suddenly imposed velocity loading. (b) The normalized displacements of the first three nodes as a function of normalized time from three different numerical methods. (c) Comparison between the asymptotic solution of Eq. (12) and simulation results.

We perform MD, explicit algorithm of FEM (ABAQUS-EXPLICIT) and implicit algorithm of FEM (ABAQUS-IMPLICIT) to simulate the dynamic response of this 1D discrete system. Fig. 3b plots the displacements of the first three nodes as a function of time. All three simulation methods predict the same displacement responses. It can be observed that all nodes respond (or start to move) at the same time when a load is imposed to the right end. We may use a specific magnitude of displacement as the threshold to detect the startup of node movement. It is found from Fig. 3b that the time intervals for adjacent nodes reaching a small displacement threshold are less than $\Delta t_{continuum}=\sqrt{m/k}$. Moreover, a lower displacement threshold corresponds to a shorter time interval. In other words, if we have a highly sensitive displacement sensor, a supersonic propagation of the non-equilibrium disturbance can be detected, a phenomenon that cannot be predicted by continuum mechanics.

At the very beginning of this dynamic process, i.e., for an infinitesimal time t, an asymptotic theoretical solution can be obtained, which can validate our simulation and demonstrate the supersonic propagation. We first investigate the relation among the dynamic responses of node i, node $i+1$ and node $i+2$ (shown in Fig. 3a) to derive a recurrence formula. The force on node $i+1$ is

$$F_{i+1}=k[u_i(t)-u_{i+1}(t)]-k[u_{i+1}(t)-u_{i+2}(t)] \tag{8}$$

where u is the displacement of node. For an infinitesimal time t, it is reasonable to assume that $|u_i(t)|\gg|u_{i+1}(t)|\gg|u_{i+2}(t)|$. Therefore, the above equation becomes

$$F_{i+1}=ku_i(t) \tag{9}$$

Dividing both sides with the node mass, the acceleration of node $i+1$ is obtained as

$$a_{i+1}(t)=\frac{d^2u_{i+1}(t)}{dt^2}=\frac{k}{m}u_i(t) \tag{10}$$

which is a recursive formula on nodal displacement.

A similar analysis predicts the displacement of node 1 as

$$u_1(t)=\frac{1}{3}\left(\frac{k}{m}\right)v_0t^3 \tag{11}$$

Together with Eq. (10), the displacement of other nodes can be computed as

$$u_n(t)=\frac{2}{(2n+1)!}\left(\frac{k}{m}\right)^n v_0t^{2n+1} \tag{12}$$

So,

$$u_2(t)=\frac{1}{60}\left(\frac{k}{m}\right)^2 v_0t^5$$

$$u_3(t)=\frac{1}{2520}\left(\frac{k}{m}\right)^3 v_0t^7 \tag{13}$$

Fig. 3c shows that this asymptotic analytical solution agrees well with the simulation results when the time t is small enough. Actually, the accuracy of the solution can be guaranteed since $u_{i+1}(t)/u_i(t)\to 0$, $u_{i+2}(t)/u_i(t)\to 0$ and Eq. (9) tends to be accurate when t approaches zero.

The asymptotic analytical solutions, Eq. (12), clearly demonstrate that all nodes move simultaneously once the load is applied at the right end, which implies the supersonic propagation of the disturbance. On the other hand, Eq. (12) also shows that the magnitude of the disturbance under supersonic propagation attenuates dramatically. After traveling over several nodes, it becomes too small to detect in reality. This can be demonstrated by the following example.

To understand the discrepancies and relations between the dynamical response of a discrete system and that predicted by continuum mechanics, we homogenize the discrete system step by step. We view the segment between the two dashed lines in Fig. 4a as one fundamental spring-mass element. One round of homogenization is realized by dividing each of such elements into three shorter elements, with three times of spring constant and one third of the node mass, as shown in Fig. 4b. Obviously, after infinite rounds of homogenization, a discrete mass-spring system transforms into a continuum bar. We investigate the effect of a series of homogenization on the displacement responses of point A with a distance d from the right end (shown in Fig. 4).

Fig. 4e plots the displacement of point A as a function of time for the original discrete system, the first three rounds of homogenized systems and the continuum bar. It is found that when a velocity load is suddenly imposed on the right end of discrete systems, point A responds at the same time. Moreover, the more homogeneous the system is, the lower the magnitude of initial response is, and the extreme case is the continuum bar, in which point A only starts to move at $t=1.5\sqrt{m/k}$, just the same as the prediction by continuum mechanics. It is also noted that if the length of concern in this example, i.e., $d=1.5l_0$, is much larger than the intrinsic length of a discrete system, i.e., the spring length l_0, the dynamical behavior can be predicted well by continuum mechanics, otherwise error may be significant.

The difference on the dynamical behavior between a discrete system and an idealized continuum solid is attributed to the fact that the massless springs in a discrete system have infinite longitudinal wave speed. All real solids are indeed

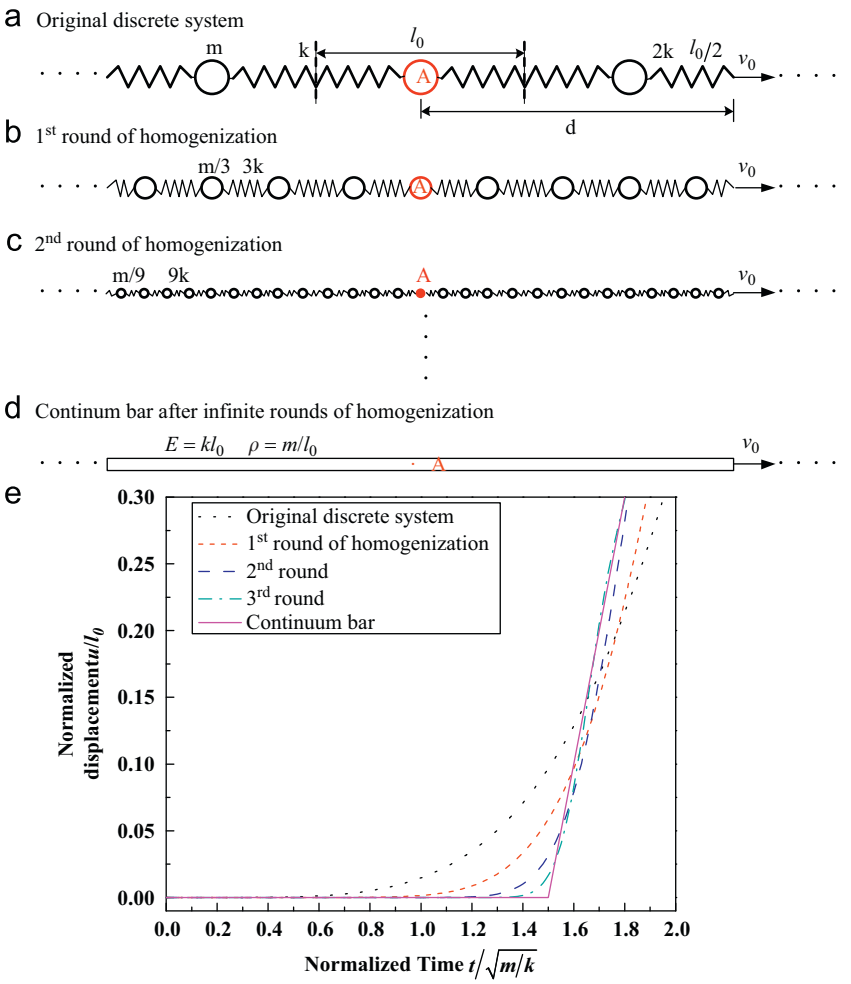

Fig. 4. Schematics of a one-dimensional discrete mass-spring system (a) and its step-by-step homogenized counterparts (b–d) subjected to a suddenly imposed velocity loading. (e) The dynamic response of point *A* for systems with different homogenity in (a–d).

discrete systems, in which no mass is related to interatomic interactions. Therefore, supersonic propagation of disturbance in real solids is possible. Because the magnitude of the supersonically propagating disturbance attenuates very quickly with the distance from the original location of the disturbance, it can hardly be detected in most situations. However, if the supersonic propagation of one non-equilibrium disturbance can trigger another disturbance and the continuous amplification of the disturbance amplitude can overbalance the amplitude attenuation, supersonic propagation of disturbance can be realized in a domino way, such as the cascade of atomic-bond breaking events occurring in the dynamic fracture process of a solid.

4. Energy supply mechanisms for supersonic crack propagation

To maintain the supersonic propagation of a non-equilibrium disturbance, one crucial requirement is a feasible energy supply mechanism, e.g., sufficient energy flow into the tip of a supersonically propagating crack. It has been demonstrated in Section 2 that supersonic crack propagation may be realized if the energy is pre-stored in front of the crack tip. In this section, we will first study the mechanism of pre-stored energy more systematically and then explore other possible energy supply mechanisms for supersonic crack propagation.

4.1. Examples with pre-stored energy in front of a supersonic crack tip

To gain a deeper understanding of the supersonic crack propagation with pre-stored energy in front of the crack tip demonstrated in Section 2 (e.g., Fig. 2d and e), we will establish a quantitative relation between the crack propagation velocity and the loading by carrying out a theoretical analysis on a four-row discrete system in this subsection.

Fig. 5a shows a four-row strip discrete system under pre-stretch, and the non-horizontal bonds have the pre-stored energy. The bonds crossing the middle plane (denoted by the dashed line) are assumed to be weak with a critical force-stretch curve shown in Fig. 1b. The crack propagates towards the right. Just after bond 1 is broken, we investigate the subsequent breaking process of bond 2 to predict the crack propagation velocity. In the regime of supersonic crack propagation, node A is in equilibrium before bond 1 breaks. During a very short time after breaking of bond 1, it is reasonable to assume that node A moves along bond 3 (denoted by the red arrow in Fig. 5a) with the acceleration

$$a=\frac{k(l_a-l_0)}{m}=\frac{3k\sigma_a l_0}{4mE'} \tag{14}$$

The time interval from the breaking of bond 1 to the breaking of bond 2, Δt, can be determined by solving the following equation:

$$\frac{1}{4}a\Delta t^2=l_c-l_a=\frac{3(\sigma_c-\sigma_a)l_0}{4E'} \tag{15}$$

and

$$\Delta t=\sqrt{\frac{4m}{k}}\sqrt{\frac{l_c-l_a}{l_a-l_0}}=\sqrt{\frac{4m}{k}}\sqrt{\frac{\sigma_c-\sigma_a}{\sigma_a}} \tag{16}$$

Therefore, the speed of the crack propagation is given by

$$v_c=\frac{l_0}{2\Delta t}=\frac{1}{3\sqrt{2}}\sqrt{\frac{l_a-l_0}{l_c-l_a}}\sqrt{\frac{E'}{\rho}}=\eta\sqrt{\frac{\sigma_a}{\sigma_c-\sigma_a}}c_l \tag{17}$$

where $\eta=1/3\sqrt{2}$ represents the effect of microstructure on the crack propagation speed and obviously depends on the angles of the triangle lattice. Eq. (17) implies that the crack propagation speed is determined by the material

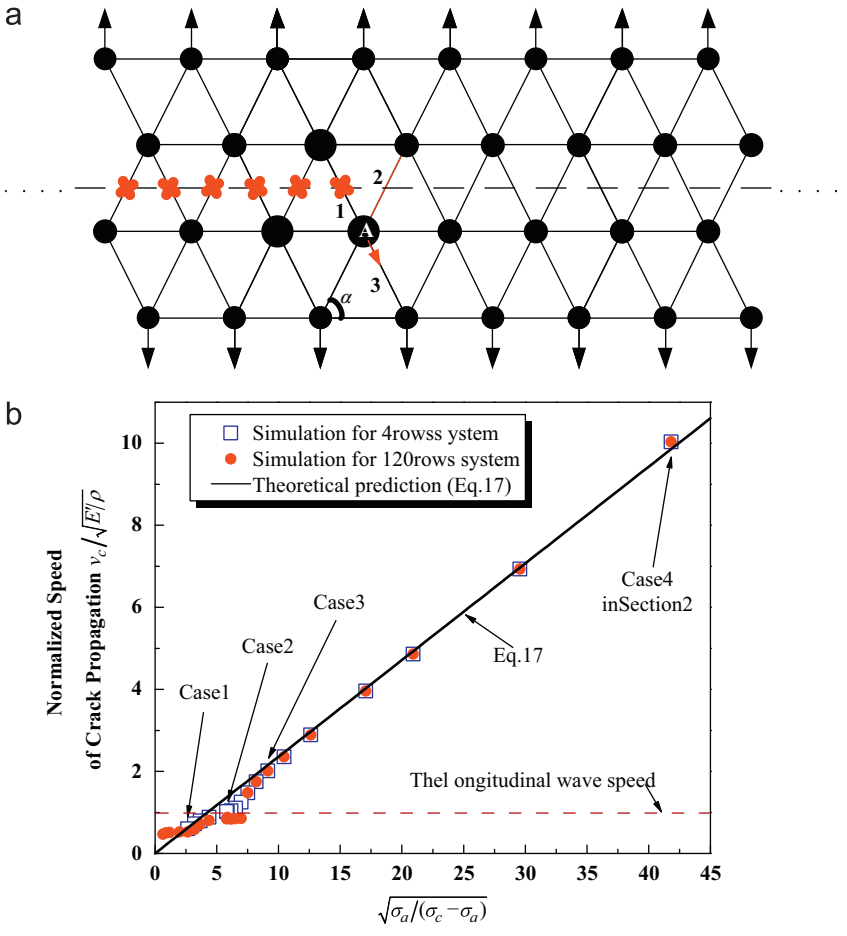

Fig. 5. (a) Schematic of a four-row strip discrete system under pre-stretch for theoretical analysis on crack propagation. (b) The normalized crack propagation velocity v_c as a function of $\sqrt{\sigma_a/(\sigma_c-\sigma_a)}$ from the theoretical prediction and simulation results.

microstructure, the stress–strength ratio and the longitudinal wave speed. Obviously, if the pre-stress σ_a is close to the bond strength σ_c, $v_c > c_l$, i.e., the crack propagation is supersonic. Fig. 5b plots normalized crack propagation velocity v_c as a function of $\sqrt{\sigma_a/(\sigma_c-\sigma_a)}$ for the theoretical prediction from Eq. (17) and the simulation results on two discrete systems (4 rows and 120 rows), respectively. The simulation results agree well with the theoretical prediction of the linear relation between v_c and $\sqrt{\sigma_a/(\sigma_c-\sigma_a)}$ in the regime of supersonic crack propagation.

We emphasize again that in the above examples, the pre-stored energy on the crack path is almost saturated, in a sense that a tiny amount of additional energy can trigger the bond breaking, which is transferred by supersonically propagating non-equilibrium disturbance from its neighbor bond breaking. As a result, supersonic crack propagation is realized.

4.2. Numerical trousers tearing experiments without pre-stored energy

In this subsection, we investigate if pre-stored energy is a necessary condition for supersonic crack propagation. Fig. 6a shows the same 4-row trousers-like discrete system and there is no pre-stretch in front of crack tip. Alternatively, we impose vertical tearing velocity loadings $v_t > c_l$ at the two ends of the trouser legs. Intuition leads to the prediction that this supersonic tearing speed might lead to supersonic crack propagation. To facilitate the tearing, an infinitesimal critical breaking strain ($(l_c-l_0)/l_0=0.00001$) is chosen for the bonds along the crack path. The simulation results are summarized in Table 1. It is found that the crack propagation velocity v_c is always lower than the longitudinal wave speed no matter how large the tearing speed v_t is. Fig. 6b shows sequential snapshots of the deformed discrete system under a tearing speed of $v_t=2c_l$, which reveals that the supersonic tearing speed leads to fast leg extension while the resulting crack propagation speed is subsonic.

The absence of supersonic crack propagation in the above example can be understood as follows. Since the velocity loadings are imposed on the fixed points far away from the crack tip, and supersonic propagation of primary energy supply from these points attenuates too quickly to provide sufficient energy flow into the crack tip. In other words, major part of the energy to drive crack propagation can only be transferred at a speed limited by the longitudinal wave speed, resulting in a subsonic crack propagation.

By contrast, if the loading points can closely follow the advancement of the crack tip, as shown in Fig. 7a, sufficient energy could reach the crack tip before significant attenuation and help maintain supersonic crack propagation. Such loading conditions can be satisfied in cases such as explosion-induced fracture and splitting wood with axe, in which inner

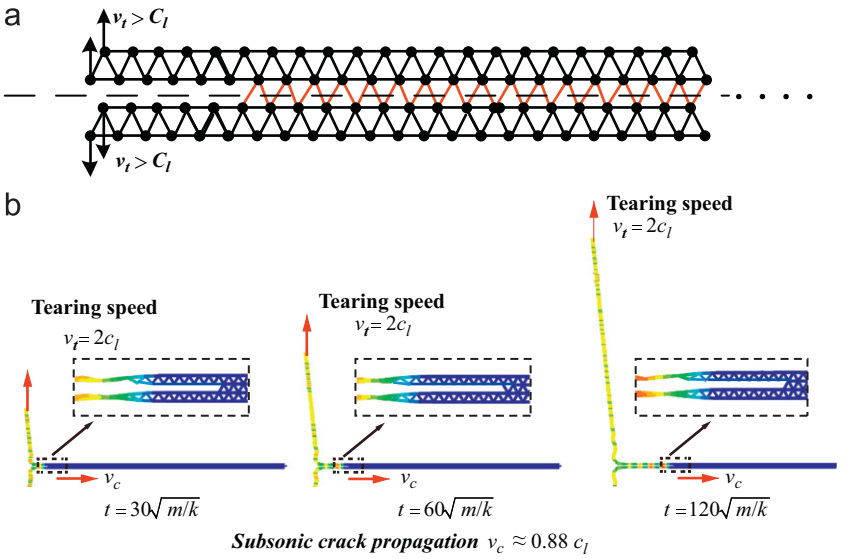

Fig. 6. Numerical trousers tearing experiments. (a) Schematic of trousers-like discrete system under tearing loadings and (b) sequential snapshots of crack propagation. Color shades denote nodal speed.

Table 1
The normalized crack propagation speeds for different normalized tearing speeds.

Tearing speed v_t/c_l	Crack propagation speed v_c/c_l
1	0.87
2	0.88
10	0.94

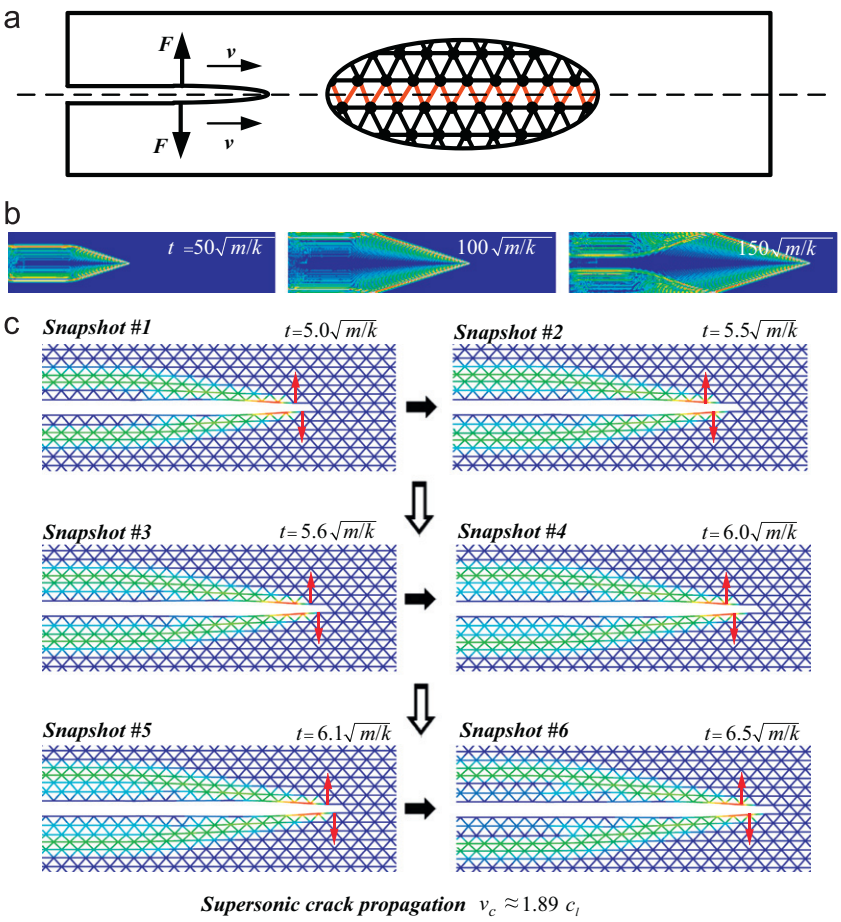

Fig. 7. (a) Schematic of a strip discrete system splitting by a pair of forces concomitantly moving with the crack tip. (b) Sequential snapshots of crack propagation. (c) Shows a close-up view of the supersonically propagating crack tip with a higher temporal resolution. Color shades denote nodal speed.

pressure is continuously imposed on the newly-formed crack surfaces. As a demonstration, a pair of moving forces $F=50kl_0$ along the vertical direction is imposed on the crack surfaces, with a fixed distance from the advancing crack tip (Fig. 7a). The same mechanical and geometrical parameters of the discrete system as in Section 2 are used here. Fig. 7b and c shows sequential snapshots of the crack propagation with two different space and time resolution. As the apparent Mach cones in Fig. 7b suggest, the crack propagation is supersonic, with a speed $v_c = 2.01 l_0\sqrt{k/m} \approx 1.89 c_l$. Therefore, supersonic crack propagation in a system without pre-stored energy is possible if there exists sufficiently large loadings that move concomitantly with the propagating crack tip.

5. Discussion

Eq. (17) suggests that the supersonic crack propagation speed not only depends on the longitudinal wave speed $c_l = \sqrt{E'/\rho}$, but also depends on the stress ratio $\sqrt{\sigma_a/(\sigma_c-\sigma_a)}$ and the microstructure geometry. However, it seems that the fracture toughness does not play a role in supersonic crack propagation. To address this issue, Section 5.1 studies the effect of the fracture toughness on crack propagation speed. The effect of microstructure geometry on supersonic crack propagation is further investigated in Section 5.2.

5.1. The effect of the fracture toughness on crack propagation speed

To investigate the influence of fracture toughness on crack propagation speed, two triangle lattice discrete systems are studied. One is the system shown in Fig. 1a and used in the simulations in previous sections. The other one has a similar lattice structure but with a longer original bond length $2l_0$. By adjusting various microscopic parameters, i.e., l_c and m, all macroscopic parameters of these two systems (e.g., the stiffness E', the density ρ, the strength σ_c, and the width of specimen h) are tailored to be the same, except the fracture toughness G_{IC}. Here the resulting ratio of the fracture toughnesses is $G_{IC}^{(2)}/G_{IC}^{(1)} \approx 2$, which is consistent with the dimensional analysis that G_{IC} is proportional to the bond length.

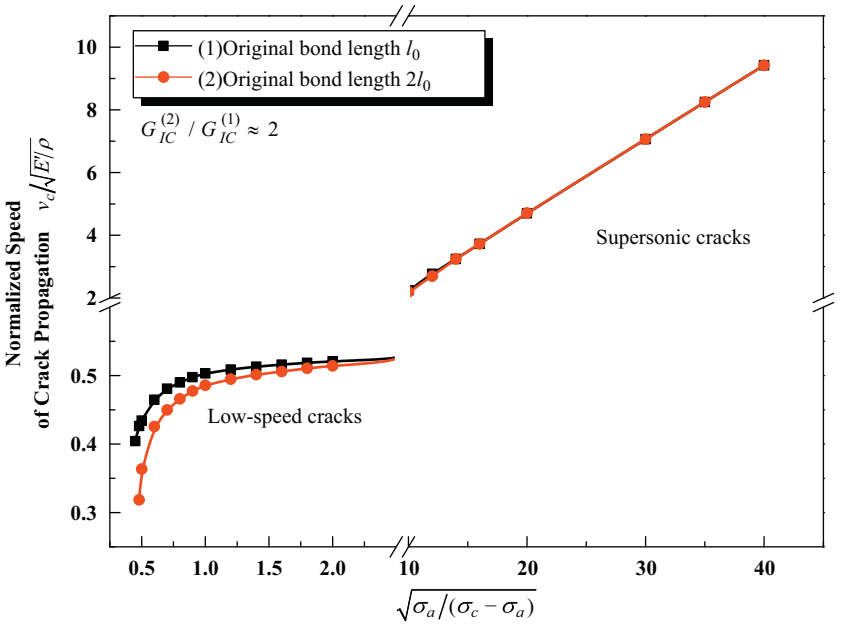

Fig. 8. The normalized crack propagation velocity v_c as a function of $\sqrt{\sigma_a/(\sigma_c-\sigma_a)}$ for two triangle systems with different fracture toughness G_{IC}.

Both systems are subject to the same applied stress σ_a as in Fig. 1a. Fig. 8 shows that the crack propagation speeds in the two systems are almost identical in the regime of supersonic propagation, which supports the theoretical prediction of Eq. (17) that supersonic propagation is independent of fracture toughness. By contrast, the crack propagation speeds in the two systems differ in the regime of subsonic crack propagation. In other words, our numerical results imply an interesting conclusion that the crack propagation speed depends on the fracture toughness in the subsonic regime, but not in the supersonic regime. This can be further understood as follows. The deformation/stress is concentrated in front of a subsonic crack (see Fig. 2b) where fracture criterion dominates, while the deformation/stress is rather uniform in front of a supersonic crack where strength criterion dominates (see Fig. 2d).

5.2. *The effect of microstructure on supersonic crack propagation*

In this subsection, we investigate the effect of microstructure (e.g., η in Eq. (17)) on supersonic crack propagation. To this end, we study the discrete systems of isosceles triangle lattice with different base angles α (see Fig. 9a), while keeping the macroscopic parameters of systems the same, including the width of model h, the nominal modulus E', the density ρ, the strength σ_c and the fracture toughness G_{IC}. To meet this requirement, other microscopic parameters of the system, including the bond length, the spring constants, and the concentrated mass, have to be adjusted. Following a similar derivation as in Section 4.1, the speed of supersonic crack propagation can be obtained as

$$v_c(\alpha) = \eta(\alpha)\sqrt{\frac{\sigma_a}{\sigma_c-\sigma_a}}\sqrt{\frac{E'}{\rho}} \tag{18}$$

where

$$\eta(\alpha) = \frac{\cos\alpha\sqrt{1-2\cos^2\alpha}}{2\sin^2\alpha} \tag{19}$$

represents the effect of microstructure on the crack propagation speed. The detailed derivation is given in the Appendix.

Fig. 9b plots the crack propagation speed as a function of the stress ratio $\sqrt{\sigma_a/(\sigma_c-\sigma_a)}$ for various microstructures, (i.e., $\alpha=75^\circ$, 67.5°, 60°, 52.5°, 47.5°). The simulation results reveal a linear dependence of crack propagation speed on the stress ratio, in excellent agreement with the analytical prediction of Eq. (18) for all microstructures considered. It is clearly shown in Fig. 9b that the microstructure does affect the supersonic crack propagation speed. Such an effect is further demonstrated by the plot of the crack propagation speed as a function of base angle for $\sqrt{\sigma_a/(\sigma_c-\sigma_a)}=40$ in Fig. 9d, which also shows an excellent agreement between simulation results and analytical prediction. Fig. 9c offers a visualized comparison of the supersonically propagating crack fronts in the five systems with various microstructures (i.e., $\alpha=75^\circ$, 67.5°, 60°, 52.5°, 47.5°) at a given instant in time.

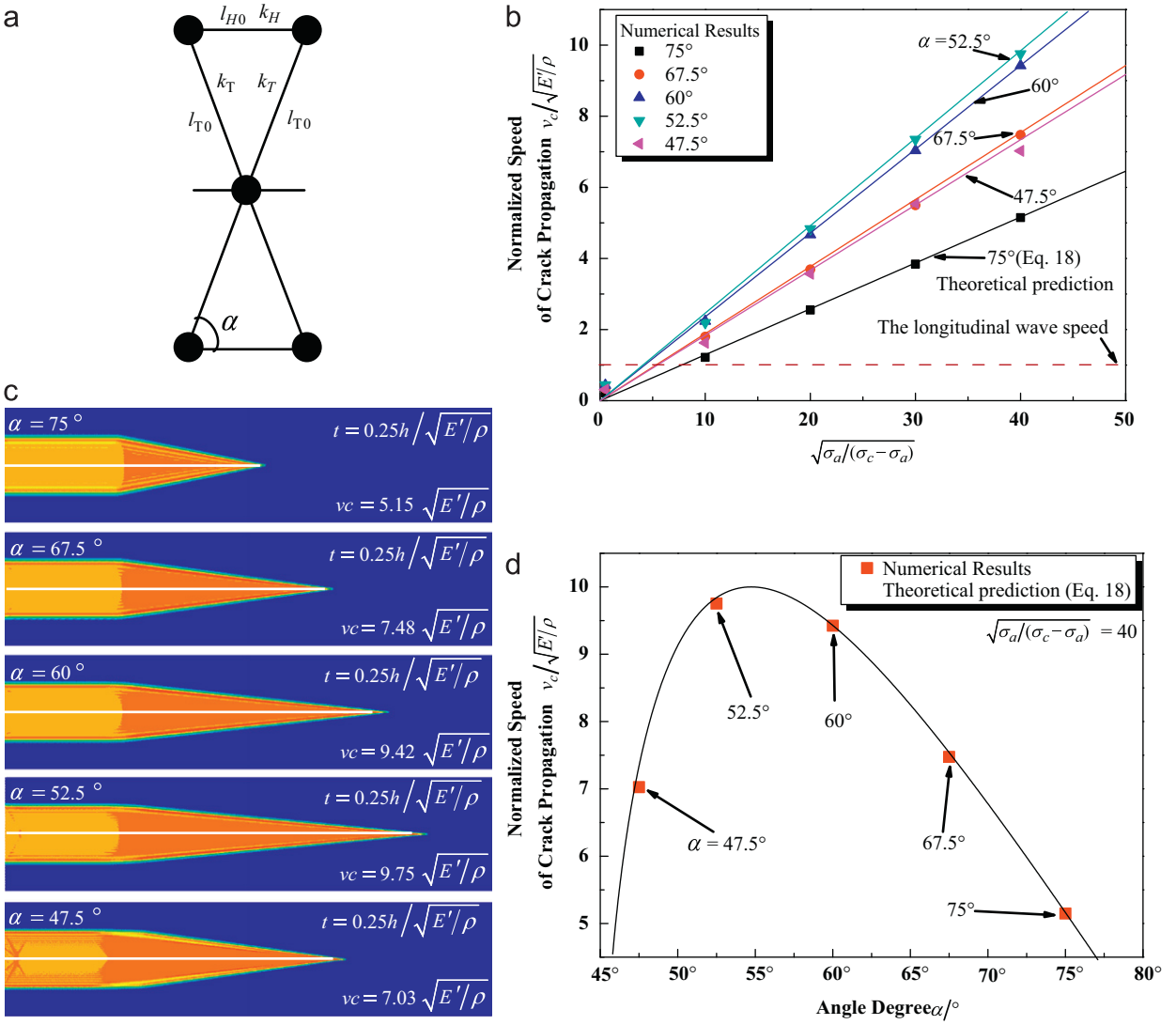

Fig. 9. (a) Schematic of a periodical unit cell of isosceles triangle lattice; The normalized crack propagation velocity v_c as functions of $\sqrt{\sigma_a/(\sigma_c-\sigma_a)}$ (b) and the base angles of isosceles triangle lattice (d). (c) Snapshots of dynamical crack fronts in pre-stretched strip specimen with different microstructures at a given instant of time. Color shades denote nodal speed.

6. Conclusions

Using theoretical analysis and numerical examples, we show that the speed of crack propagation in solids is not limited by the longitudinal wave speed. We further quantitatively relate the speed of supersonic crack propagation with both material properties and microstructure parameters. The following conclusions can be drawn:

(1) Non-equilibrium disturbance (e.g. force, displacement, energy, and so on) can propagate at a supersonic speed in discrete systems, in contrast to the prediction of continuum mechanics, in which no information can propagate faster than the longitudinal wave speed. Since all solids are essentially discrete atomic systems, supersonic propagation of disturbance is indeed possible. The magnitude of non-equilibrium disturbances during supersonic propagation, however, attenuates very quickly; as a result, it can hardly be observed in reality.

(2) In a dynamic fracture process, the supersonic propagation of one non-equilibrium disturbance can trigger another disturbance, i.e., a cascade of atomic-bond breaking events, which serves as an amplification mechanism to counterbalance the attenuation of the disturbance. Consequently, supersonic crack propagation can be realized in a domino way.

(3) Another key factor for supersonic crack propagation is to ensure sufficient energy flow into the crack tip. Nevertheless, it is found that the major part of energy can only be transferred at a speed limited by the longitudinal wave speed.

Therefore, the conditions for the occurrence of supersonic crack propagation can hardly be met in most situations, unless there exists sufficiently high pre-stored energy along the crack path or continuous energy supply from the loadings concomitantly moving with the crack tip.

(4) The study on the triangle lattice systems shows that, supersonic crack propagation speed not only depends on the longitudinal wave speed $c_l=\sqrt{E'/\rho}$ and the stress–strength ratio $\sqrt{\sigma_a/(\sigma_c-\sigma_a)}$, but also on the microstructure geometry, which implies that macroscopic quantities cannot fully determine the supersonic crack speed. Moreover, it is interesting to note that the fracture toughness only affects the crack propagation speed in the subsonic regime, but not in the supersonic regime, since the deformation/stress is uniform in front of a supersonic crack where strength criterion dominates.

Acknowledgment

BL, YJJ and WPZ acknowledge the support from National Natural Science Foundation of China (Grant nos. 11090334, 10732050, 90816006, and 10820101048), National Basic Research Program of China (973 Program Grant nos. 2007CB936803 and 2010CB832701), and the support from Tsinghua University Initiative Scientific Research Program (no. 2011Z02173). TL acknowledges the support of US National Science Foundation (under Grants 0856540 and 0928278).

Appendix

To ensure that the macroscopic parameters of different isosceles triangle lattices are the same as those for the equilateral triangle lattice, we perform the theoretical analysis on the representative periodical unit shown in Fig. A1.

From the geometric relations in Fig. A1a, it is found that

$$l_{H0}=2\cos\alpha\, l_{T0} \tag{A1}$$

where l_{H0} and l_{T0} represent the original bond length of horizontal and tilted bonds, respectively.

After infinitesimal biaxial stretching, as shown in Fig. A1b, the bond lengths of deformed periodical unit can be computed as,

$$\begin{aligned} l_H &= 2(1+\varepsilon_{11})\cos\alpha l_{T0} \\ l_T &= (1+\cos^2\alpha\,\varepsilon_{11}+\sin^2\alpha\,\varepsilon_{22})l_{T0} \end{aligned} \tag{A2}$$

The equivalent stresses in deformed configuration can be expressed as

$$\begin{aligned} \sigma_{11} &= \frac{k_H(l_H-l_{HO})+k_T(l_T-l_{TO})\cos\alpha}{\sin\alpha l_{T0}} \\ \sigma_{22} &= \frac{k_T(l_T-l_{TO})\sin\alpha}{\cos\alpha\, l_{TO}} \end{aligned} \tag{A3}$$

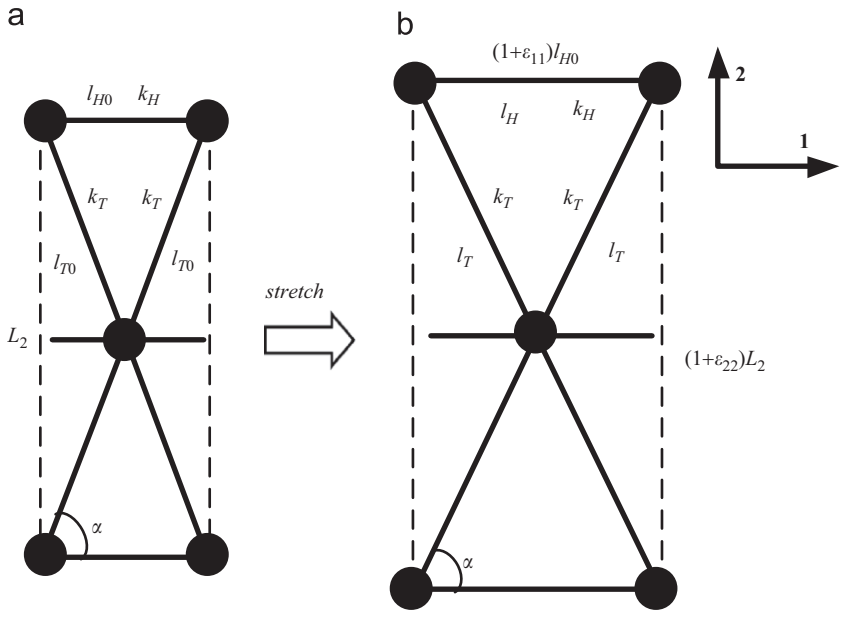

Fig. A1. Schematics of (a) an undeformed and (b) a deformed periodical unit cell of isosceles triangle lattice for theoretical analysis.

Substituting Eq. (A2) into Eq. (A3) yields

$$\sigma_{11} = \frac{\cos\alpha}{\sin\alpha}(2k_H + \cos^2\alpha k_T)\varepsilon_{11} + \sin\alpha\cos\alpha k_T\varepsilon_{22}$$

$$\sigma_{22} = \sin\alpha\cos\alpha\, k_T\varepsilon_{11} + \frac{\sin^3\alpha}{\cos\alpha}k_T\varepsilon_{22} \tag{A4}$$

Since the 1-direction displacements on the upper and lower boundaries of the strip specimen are fixed in our simulation, the following nominal moduli can represent the stiffness better than Young's modulus,

$$E'_{11} = \left.\frac{\sigma_{11}}{\varepsilon_{11}}\right|_{\varepsilon_{22}=0} = \frac{2\cos\alpha\, k_H + \cos^3\alpha\, k_T}{\sin\alpha} \tag{A5}$$

$$E'_{22} = \left.\frac{\sigma_{22}}{\varepsilon_{22}}\right|_{\varepsilon_{11}=0} = \frac{\sin^3\alpha\, k_T}{\cos\alpha} \tag{A6}$$

Noting that the equilateral triangle lattice has isotropic modulus, we let $E'_{11} = E'_{22} = E'$ for the isosceles triangle lattice and obtain

$$2\cos^2\alpha k_H = (1-2\cos^2\alpha)k_T \tag{A7}$$

Substituting Eq. (A7) into Eqs. (A5) and (A6) k_H and k_T can be determined as

$$k_H = \frac{1-2\cos^2\alpha}{2\cos\alpha\sin^3\alpha}E'$$

$$k_T = \frac{\cos\alpha}{\sin^3\alpha}E' \tag{A8}$$

Eq. (A7) implies that the range of α is from 45° to 90°.

Our numerical simulations on the isosceles triangle lattice indicate that the longitudinal wave speed is still $\sqrt{E'/\rho}$. The fracture toughness of the strip system can be computed as

$$G_{IC} = \frac{1}{2}E'\varepsilon_{kc}^2 h \tag{A9}$$

where h is the width of the system, ε_{kc} is the strain far ahead of the crack at which the crack begins to propagate.

Similar to the derivation as illustrated in Fig. 5a, the analysis on the supersonic crack propagation speed is given as follows. We denote the strength and pre-stress of the system as σ_c and σ_a. The fracture length and pre-stretch length of bonds are l_{Tc} and l_{Ta}. From Eq. (A2), the acceleration of point A can be computed as

$$a = \frac{k_T(l_{Ta}-l_{T0})}{m} = \frac{k_T}{m}\sin^2\alpha\frac{\sigma_a}{E'}l_{T0} \tag{A10}$$

where the mass of A is

$$m = 2\rho(l_{T0})^2\sin\alpha\cos\alpha$$

The time interval from the breaking of bond 1 to the breaking of bond 2, Δt, can be determined by solving the following equation:

$$\frac{1}{2}a(1-2\cos^2\alpha)\Delta t^2 = l_{Tc}-l_{Ta} = \sin^2\alpha\frac{\sigma_c-\sigma_a}{E'}l_{T0} \tag{A11}$$

Therefore, the speed of the crack propagation is given by

$$v_c(\alpha) = \frac{l_{H0}}{2\Delta t} = \eta(\alpha)\sqrt{\frac{\sigma_a}{\sigma_c-\sigma_a}}\sqrt{\frac{E'}{\rho}} \tag{A12}$$

where

$$\eta(\alpha) = \frac{\cos\alpha\sqrt{1-2\cos^2\alpha}}{2\sin^2\alpha} \tag{A13}$$

represents the effect of microstructure on the crack propagation speed.

References

ABAQUS, 2005. ABAQUS Theory Manual and Users Manual, version 6.5, Hibbit, Karlsson and Sorensen, Pawtucket, RI.
Abraham, F.F., 1996. Dynamics of brittle fracture with variable elasticity. Phys. Rev. Lett. 77, 272–275.
Abraham, F.F., 1997. Instability dynamics in three-dimensional fracture: an atomistic simulation. J. Mech. Phys. Solids 45, 1461–1471.
Abraham, F.F., 2001. The atomic dynamics of fracture. J. Mech. Phys. Solids 49, 2095–2111.
Abraham, F.F., Brodbeck, D., Rudge, W.E., Xu, X., 1994. Instability of fracture—a computer-simulation investigation. Phys. Rev. Lett. 73, 272–275.

Abraham, F.F., Brodbeck, D., Rudge, W.E., Xu, X., 1997. A molecular-dynamics investigation of rapid fracture mechanics. J. Mech. Phys. Solids 45, 1595–1619.
Abraham, F.F., Gao, H., 2000. How fast can cracks propagate? Phys. Rev. Lett. 84, 3113–3116.
Andrews, D.J., 1976. Rupture velocity of plane strain shear cracks. J. Geophys. Res. 81, 5679–5687.
Broberg, B., 1999. In: Cracks and FractureAcademic, San Diego 1999.
Buehler, M.J., Abraham, F.F., Gao, H., 2003. Hyperelasticity governs dynamic fracture at a critical length scale. Nature 426, 141–146.
Buehler, M.J., Abraham, F.F., Gao, H., 2004a. Multiscale Modeling and Simulation, 143–156.
Buehler, M.J., Gao, H.J., 2006. Dynamical fracture instabilities due to local hyperelasticity at crack tips. Nature 439, 307–310.
Buehler, M.J., Gao, H.J., Huang, Y.G., 2004b. Atomistic and continuum studies of stress and strain fields near a rapidly propagating crack in a harmonic lattice. Theor. Appl. Fract. Mech. 41, 21–42.
Burridge, R., 1973. Admissible speeds for plane-strain self-similar shear cracks with friction but lacking cohesion. Geophys. J. R. Astronomical Soc. 35, 439–455.
Cramer, T., Wanner, A., Gumbsch, P., 2000. Energy dissipation and path instabilities in dynamic fracture of silicon single crystals. Phys. Rev. Lett. 85, 788–791.
Fineberg, J., Gross, S.P., Marder, M., Swinney, H.L., 1991. Instability in dynamic fracture. Phys. Rev. Lett. 67, 141–144.
Freund, L.B., 1998. In: Dynamic Fracture MechanicsCambridge Univ. Press, Cambridge, UK 1998.
Gao, H., 1996. A theory of local limiting speed in dynamic fracture. J. Mech. Phys. Solids 44, 1453–1474.
Gao, H., 1997. Elastic eaves in a hyperelastic solid near its plane-strain equibiaxial cohesive limit. Philos. Magn. Lett. 76, 307–314.
Gao, H.J., Huang, Y.G., Abraham, F.F., 2001. Continuum and atomistic studies of intersonic crack propagation. J. Mech. Phys. Solids 49, 2113–2132.
Guo, G.F., Yang, W., Huang, Y., 2003. Supersonic crack growth in a solid of upturn stress–strain relation under anti-plane shear. J. Mech. Phys. Solids 51, 1971–1985.
Guozden, T., Jagla, E., Marder, M., 2010. Supersonic cracks in lattice models. Int. J. Fract 162, 107–125.
Guozden, T.M., Jagla, E.A., 2005. Supersonic crack propagation in a class of lattice models of mode III brittle fracture. Phys. Rev. Lett., 95.
Hauch, J.A., Holland, D., Marder, M.P., Swinney, H.L., 1999. Dynamic fracture in single crystal silicon. Phys. Rev. Lett. 82, 3823–3826.
Hauch, J.A., Marder, M.P., 1998. Energy balance in dynamic fracture, investigated by a potential drop technique. Int. J. Fracture 90, 133–151.
Marder, M., Gross, S., 1995. Origin of crack-tip instabilities. J. Mech. Phys. Solids 43, 1–48.
Mishuris, G.S., Movchan, A.B., Slepyan, L.I., 2008. Dynamics of a bridged crack in a discrete lattice. Quarterly J Mech. Appl. Math. 61, 151–160.
Mishuris, G.S., Movchan, A.B., Slepyan, L.I., 2009. In: Silberschmidt, V.V. (Ed.), Localization and dynamic defects in lattice structures. Computational and experimental mechanics of advanced materials, Springer, Vienna, pp. 51–82.
Needleman, A., 1999. An analysis of intersonic crack growth under shear loading. J. Appl. Mech.-Trans. Asme 66, 847–857.
Petersan, P.J., Deegan, R.D., Marder, M., Swinney, H.L., 2004. Cracks in rubber under tension exceed the shear wave speed. Phys. Rev. Lett., 93.
Ravi-Chandar, K., 1998. Dynamic fracture of nominally brittle materials. Int. J. Fracture 90, 83–102.
Rosakis, A.J., 2002. Intersonic shear cracks and fault ruptures. Adv. Phys. 51, 1189–1257.
Rosakis, A.J., Samudrala, O., Coker, D., 1999. Cracks faster than the shear wave speed. Science 284, 1337–1340.
Rountree, C.L., 2002. Atomistic aspects of crack propagation in brittle materials: multimillion atom molecular-dynamics simulations. Annu. Rev. Mater. Res. 32, 377–400.
Slepyan, L.I., 1972. Nonstationary elastic waves. Sudostroenie, Leningrad (in Russian).
Slepyan, L.I., 1981. Crack propagation in high-frequency lattice vibrations. Sov. Phys.-Dokl 26, 900–902902.
Slepyan, L.I., 2001a. Feeding and dissipative waves in fracture and phase transition. III. Triangular-cell lattice. J. Mech. Phys. Solids 49, 2839–2875.
Slepyan, L.I., 2001b. Feeding and dissipative waves in fracture and phase transition: I. Some 1D structures and a square-cell lattice. J. Mech. Phys. Solids 49, 469–511.
Slepyan, L.I., 2002. In: Models and Phenomena in Fracture Mechanics, Springer, Berlin 2002.
Swadener, J.G., Baskes, M.I., Nastasi, M., 2002. Molecular dynamics simulation of brittle fracture in silicon. Phys. Rev. Lett. 89, 085503.